

## Non-schubart periodic orbits in the rectilinear three-body problem

Masaya Masayoshi Saito · Kiyotaka Tanikawa

Received: 23 September 2009 / Revised: 9 March 2010 / Accepted: 19 April 2010 /

Published online: 26 May 2010

© Springer Science+Business Media B.V. 2010

**Abstract** In the present paper, in the rectilinear three-body problem, we qualitatively follow the positions of non-Schubart periodic orbits as the mass parameter changes. This is done by constructing their characteristic curves. In order to construct characteristic curves, we assume a set of properties on the shape of areas corresponding to symbol sequences. These properties are assured by our preceding numerical calculations. The main result is that characteristic curves always start at triple collision and end at triple collision. This may give us some insight into the nature of periodic orbits in the  $N$ -body problem.

**Keywords** Chaos · Periodic orbits · Symbolic dynamics · Three-body problem · Triple collision

### 1 Introduction

The three-body problem is still fascinating to researches in spite of its old formulation. From the astronomical view, it is studied as a simplest model of planetary/stellar systems (Giorgilli et al. 2009; Topputo and BelBruno 2009), whereas it gives researches of dynamical systems a sound example of chaotic system having its origin in the real world. A certain restricted initial conditions for which three bodies are keeping a special configuration are considered in studies for the latter interest (Kovács and Érdi 2009; Gidea and Llibre 2010).

In the case of our system, three bodies are located on a line. This problem, called the rectilinear three-body problem, has been extensively studied (Mikkola and Hietarinta 1989; Hietarinta and Mikkola 1993; Tanikawa and Mikkola 2000a; Tanikawa and Mikkola 2000b)

---

M. M. Saito (✉)

The Institute of Statistical Mathematics, Midoricho 10-3, Tachikawa, Tokyo 190-0014, Japan  
e-mail: saitohm@ism.ac.jp

K. Tanikawa

Division of Theoretical Astronomy, National Astronomical Observatory of Japan,  
Osawa 2-21-1, Mitaka, Tokyo 181-8588, Japan  
e-mail: tanikawa.ky@nao.ac.jp

and recent progress is reviewed in [Orlov et al. \(2009\)](#). The present paper is the third of our works on this system ([Saito and Tanikawa 2007](#); [Saito and Tanikawa 2009](#)) referred to as Papers I and II). We have been interested in the behaviour of periodic orbits when the mass parameter is changed. As has been shown in Paper II, periodic orbits bifurcated from the Schubart orbit recede from the mother orbit and move toward the triple collision manifold with the change of parameter. However, we could not prove that these actually arrive at the manifold. On the other hand, in Paper II, we found a non-Schubart orbit with a stable island of non-negligible size and with symbol sequence  $(21121)^\infty$ . We found that this orbit is born through saddle-node bifurcation. Paper II suggested that its characteristic curve should arrive at triple collision. Here by a characteristic curve, we mean a locus of periodic points in the three dimensional space, that is, a direct product of the Poincaré section and the mass parameter space (see §3.3 for a detail).

In the present paper, in order to confirm the suggestion of Paper II, we follow the movement of non-Schubart periodic orbits. In other words, we determine the qualitative shape of their characteristic curves. A characteristic curve is constructed by connecting the locations of periodic points at respective mass parameters. Locations of periodic points are specified as an intersection of two areas of arch-shaped band representing respectively the future and past periodic cylinder set of symbol sequences. Since our purpose is qualitative, we abstract certain properties on the shape of areas from numerical results of Paper I. Most important property is that these band-areas have convergence points at triple collision manifold.

Our main result is that characteristic curves always start at triple collision and end at triple collision, at least in the cases of our study. Our approach is expected to be applicable to general periodic orbits except for the Schubart orbit and its daughters. We want to comment that the essential event in the bifurcation of non-Schubart periodic orbit is not saddle-node bifurcation but triple collision.

## 2 Preparation

### 2.1 Equations of motion and Poincaré section

The Hamiltonian of the rectilinear three-body problem is

$$H = \left[ \frac{1}{2} \left( \frac{1}{m_1} + \frac{1}{m_0} \right) p_1^2 + \frac{1}{2} \left( \frac{1}{m_0} + \frac{1}{m_2} \right) p_2^2 - \frac{p_1 p_2}{m_0} \right] - \left[ \frac{m_1 m_0}{q_1} + \frac{m_0 m_2}{q_2} + \frac{m_1 m_2}{q_1 + q_2} \right], \quad (1)$$

where we denote the left, center, and right particles and their masses by  $m_1$ ,  $m_0$ , and  $m_2$ , and the distances  $\overline{m_1 m_0}$  and  $\overline{m_0 m_2}$  by  $q_1$  and  $q_2$ . Following Paper II, we restrict ourselves to the cases with total energy  $E = -1$  and a symmetric mass configuration  $m_1 = m_2$ . We normalise the total mass to 3 and introduce a mass parameter  $a$  defined as  $m_1 = m_2 = 1 - a$  and  $m_0 = 1 + 2a$ . In order to study the structure of the phase space of this system, we use the Poincaré section  $\prod_{\text{all}} = \{(\theta, R) | 0 \leq \theta < 360^\circ, 0 \leq R \leq R_{\max}\}$ , which is first introduced by [Mikkola and Hietarinta \(1989\)](#). The following is a minimal description of this section. The parameter  $R \equiv (q_1 + q_2)/2$  determines the scale of the system, whose maximum  $R_{\max}$  depends on  $E$  and  $a$ . Parameter  $\theta$  is the angular variable and distributes the velocity between  $\dot{q}_1$  and  $\dot{q}_2$  for a given kinetic energy.

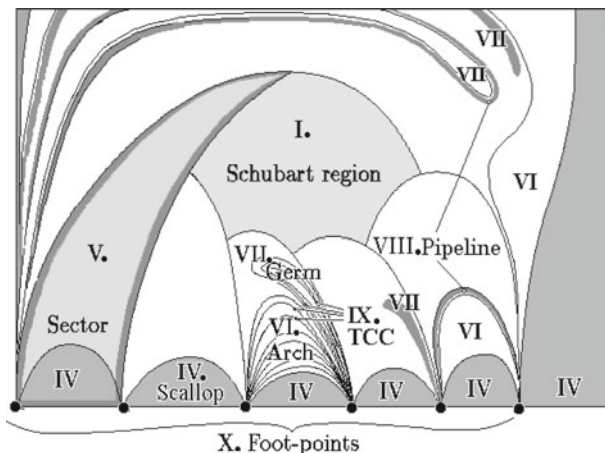


**Fig. 1** The schematic illustration of the structure on the Poincaré section. The Poincaré section consists of the Schubart region (*I*) and sectors (*V*). The sector (*V*) include one scallop (*IV*), one arch (*VI*), and optional germs (*VII*) and pipelines (*VIII*). In the third sector from the *left*, it is shown that both an arch and a germ consist of the strata of triple collision curves. In the blank area of this sector, there are other germs and/or pipelines. The pipeline (*VIII*) is an object which connects two germs in different sectors (Reproduction of Fig. 2 in Paper I)

## 2.2 Symbolic sequence and related notations

Tanikawa and Mikkola (2000b) introduced symbol sequences. Following them, we assign ‘1’ to collision between  $m_1$  and  $m_0$ , ‘2’ to collision between  $m_0$  and  $m_2$ , and ‘0’ to triple collision and describe an orbit as a sequence of symbols arranged in the order of time. Symbol sequences are split by ‘.’ and the left and the right sides correspond to the past and future sequences of collisions.

We introduce several notations related to symbol sequences as follows. A finite or infinite sequence of symbols is called a *word* and a set of symbol sequences which share a fixed word is called a *cylinder set* or just a *cylinder*. Arbitrary words, denoted by ‘\*’, are used for the definition of cylinder sets (e.g.  $\{*(.21)^n*\mid n \geq 3\}$ ). The symbol sequence for initial condition  $p \in \prod_{\text{all}}$  is denoted by  $\text{seq } p$ , and its past and future parts by  $\text{seq}_- p$  and  $\text{seq}_+ p$ . Finally, the region on  $\prod_{\text{all}}$  corresponding to a given set  $C$  of symbol sequences is denoted by  $[\![C]\!]$  namely  $[\![C]\!] = \{p \in \prod_{\text{all}} \mid \text{seq } p \in C\}$ .

## 3 Cylinder and periodic orbits

### 3.1 Structure of the surface of section

We explained the schematic structure of the surface of section in Papers I and II (see Fig. 1). In the present work, we are interested in region VI, i.e., the arch. This region consists of an infinite number of sub-arches, all of which are bounded by two triple-collision curves. Triple-collision curves have two foot-points on the  $\theta$ -axis. So, sub-arches are of thin crescent form with their tips on the  $\theta$ -axis.

As mass parameter  $a$  decreases, foot-points move to the left, and at each total degeneracy, a new foot-point is added, hence the number of sectors increase by one. Sub-arches at the

lowest position simply move to the left. We call these the persistent sub-arches. Sub-arches at higher positions change their position from a sector to another during one total degeneracy to the next. These sub-arches metamorphose themselves into pipelines and germs during the change of positions.

### 3.2 Existence of periodic sequences and periodic orbits

In this section, we introduce set operations on  $\prod_{\text{all}}$ , through which we obtain regions where periodic orbits exist. Any periodic orbit has a sequence of the form  $w^\infty.w^\infty$  with word  $w$  of length greater than one. We hereafter call  $w$  the *periodic word* of a periodic sequence  $w^\infty.w^\infty$ . A periodic sequence does not mean that the orbit is periodic, but the orbital points of this periodic orbit are contained in  $\llbracket \{w^\infty.w^\infty\} \rrbracket$ . In the present study, we assume that region  $\llbracket \{w^\infty.w^\infty\} \rrbracket$  has a periodic point. It is justified, if the map from  $\llbracket \{w^\infty.w^\infty\} \rrbracket$  onto itself to be a *twist map*.

The equality  $\llbracket \{w^\infty.w^\infty\} \rrbracket = \llbracket \{w^\infty.*\} \rrbracket \cap \llbracket *.*w^\infty \rrbracket$  shows that the region of the left-hand side is obtained as an intersection of two regions corresponding to the past and the future cylinders. In symmetric mass configurations, the past cylinder is obtained from the future cylinder owing to Theorem 1. We need some notations. Let  $w = c_1 \dots c_n$  be an arbitrary word of length  $n > 0$ . We define  $w^T$  and  $\bar{w}$  by  $(c_1 \dots c_n)^T = (c_n \dots c_1)$  and  $\overline{c_1 \dots c_n} = \bar{c}_1 \dots \bar{c}_n$  with  $\bar{1} = 2$ ,  $\bar{2} = 1$ , and  $\bar{0} = 0$ .

**Theorem 1** (Tanikawa and Mikkola 2000a) *The following symmetry (a) is always satisfied, and symmetry (b) is satisfied in the symmetric mass configuration.*

- (a)  $\text{seq}_\pm(\theta, R) = (\overline{\text{seq}_\mp(\theta + 180^\circ, R)})^T$ , for  $0^\circ \leq \theta < 180^\circ$
- (b)  $\text{seq}_\pm(\theta, R) = (\overline{\text{seq}_\mp(180^\circ - \theta, R)})^T$ , for  $0^\circ \leq \theta < 90^\circ$

Due to this theorem, we need to consider only the half of  $\prod_{\text{all}}$ ,  $\Pi = \{(\theta, R) | 0^\circ \leq \theta < 180^\circ, 0 \leq R \leq R_{\max}\}$ . Symmetry (b) is rewritten as a statement with respect to the region on  $\Pi$ :

- (b')  $\llbracket v.w \rrbracket = \mathcal{M} \llbracket \bar{w}^T \cdot \bar{v}^T \rrbracket$  where  $\mathcal{M}(\theta, R) = (180^\circ - \theta, R)$  and  $v, w$  are semi-infinite words.

The following theorem allows us to determine the location of periodic points in a desired accuracy from symbol sequences truncated at a finite digit:

**Theorem 2** *Let  $D_1^+ = \llbracket *.w* \rrbracket$  and  $D_1^- = \llbracket *w.* \rrbracket$  be sub-arches. There exist  $D_\infty = \llbracket w^\infty.w^\infty \rrbracket$ , if  $D_1 = D_1^+ \cap D_1^- \neq \emptyset$  and if this intersection is transverse.*

*Proof* An orbit with initial condition  $x_0 \in \llbracket *w.w* \rrbracket$  can be translated by proper time shifts to orbits with initial conditions  $x_- \in \llbracket *w^2.* \rrbracket \equiv D_2^-$  and  $x_+ \in \llbracket *.w^2* \rrbracket \equiv D_2^+$ . Since  $D_2^\pm \subset D_1^\pm$  and the form of  $D_2^\pm$  is similar to that of  $D_1^\pm$  (that is,  $D_2^\pm$  are sub-arches contained in sub-arches  $D_1^\pm$ ),  $D_2^+$  and  $D_2^-$  intersect transversely. Similarly,  $D_n^+ = \llbracket *.w^n* \rrbracket$  and  $D_n^- = \llbracket *w^n.* \rrbracket$  intersect transversely. As a limit, we have  $\llbracket w^\infty.w^\infty \rrbracket = D_+^\infty \cap D_-^\infty \neq \emptyset$  since  $D_n^\pm$  are closed.

### 3.3 Characteristic curves

Cylinder sets are realised as objects taking various shapes such as arches, germs, and pipelines (See Fig. 1) in the surface of section  $\Pi$ . We concentrate our attention to persistent arches.

Suppose that there is a word  $w_n$  of length  $n$ , and that arches  $\mathcal{A}_+ \equiv [[\{*.w_n*\}]]$  and  $\mathcal{A}_- \equiv [[\{*w_n.*\}]]$  are realised on  $\Pi$ . Then, we have  $\mathcal{A}_- = \mathcal{M} [[\{*.w_n^T*\}]] \equiv \mathcal{M} \mathcal{B}_+$  and  $[[w_n^\infty.w_n^\infty]] \subset \mathcal{A}_+ \cap \mathcal{A}_-$ , according to Theorem 1 (b') and Theorem 2, respectively. Future symbol sequences were obtained in Paper I and then it was observed that arches, such as  $\mathcal{A}_+$  and  $\mathcal{B}_+$ , move to the left in the surface  $\Pi$  as parameter  $a$  goes down; in turn  $\mathcal{A}_-$  moves to the right; consequently,  $\mathcal{A}_+ \cap \mathcal{A}_-$  generally changes positions. This means that, in the  $(a, \Pi)$ -space, positions of periodic orbits make curves. These are called *characteristic curves*. We will project these curves on the  $(a, R)$ -space, which we also call characteristic curves.

In the next section, we construct characteristic curves.

## 4 Characteristic curves of periodic orbits

### 4.1 Shape and configuration of persistent arches

Shapes of characteristic curves depends on those of  $\mathcal{A}_+$  and  $\mathcal{A}_-$ . These (persistent) arches have foot-points on the  $\theta$ -axis. For simplicity, we consider that arches can be modelled by truncated parabolas which are parametrised by three quantities: the height (from the  $\theta$ -axis), width (stride between foot-points), slant (inclination of the axis of the parabola). We cannot exhaust all possible cases of the form of arches, because there are too many combinations of three parameters. We will be content with treating typical four cases in what follows.

*Case 1: “face to face”* This is the case of Fig. 2a and b: The right-going arch (RG-arch) is slanted to the right and the left-going arch (LG-arch) is slanted to the left. Two sub-cases 1A and 1B are considered: the taller and wider arch versus the shorter and narrower one (the case of Fig. 2a) and the taller and narrower vs the shorter and wider (the case of Fig. 2b).

*Case 2: “face to back”* This is the case of Fig. 2c, d, and e: Both of the arches are slanted to the right.

*Case 3: “double bells”* This is the case of Fig. 2f: Both of arches are unslanted.

*Case 4: “back to back”* This is the case of Fig. 2h: the RG-arch is slanted to the left and the LG-arch is slanted to the right. This case is identical to case 1 if the change of parameter  $a$  is reversed. Figure 2 shows the counter part of case 1A.

### 4.2 Construction of characteristic curves

In this section, we try to qualitatively obtain the shape of characteristic curves. We begin with remarks on special events that occur when two arches pass through each other:

- a. The first (resp. last) intersection takes place at a terminal of parabola (a foot-point of an arch) or some other points. The intersection is transversal in the former case, whereas tangential in the latter case.
- b. There can be four tangential intersections, which are analogous to the case of total solar eclipse. These contacts are called the first, second, third, and fourth ones in the order of the events. We borrow this terminology to our problems.

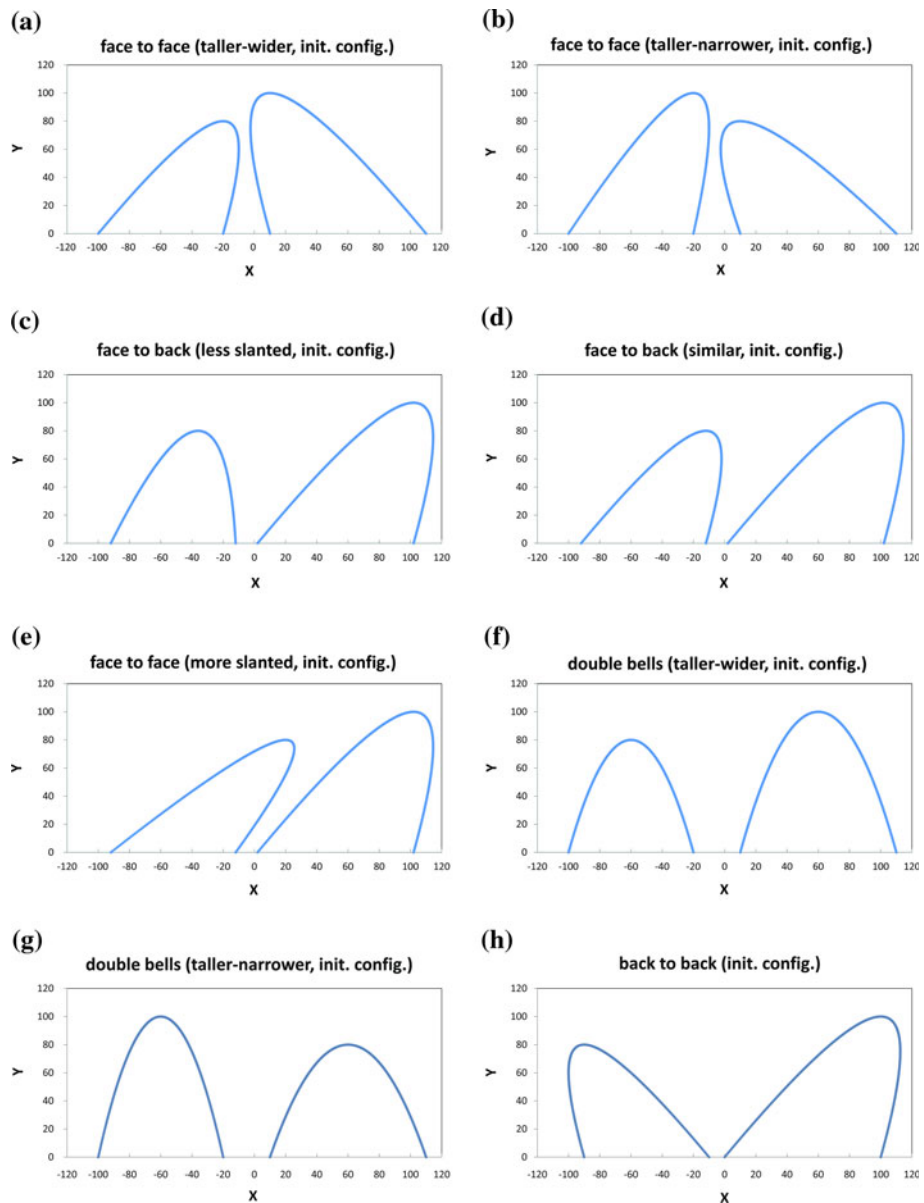


**Fig. 2** Configuration of two slanted parabolas which simulate arches. The coordinates ( $X, Y$ ) correspond to  $(\theta, R)$  of the surface of section. **a** Case 1A. **b** Case 1B. **c** Case 2A. **d** Case 2B. **e** Case 2C. **f** Case 3A. **g** Case 3B. **h** Case 4A

- c. As we will see, the characteristic curve generally has two components. This is obvious in the case where the larger arch totally encloses the smaller arch.
- d. A saddle-node bifurcation of periodic points occurs in the case of tangential intersection.

Case 1 is the easiest to understand of all events, so we describe this case in detail. As for the other cases, we briefly remark on differences from Case 1.

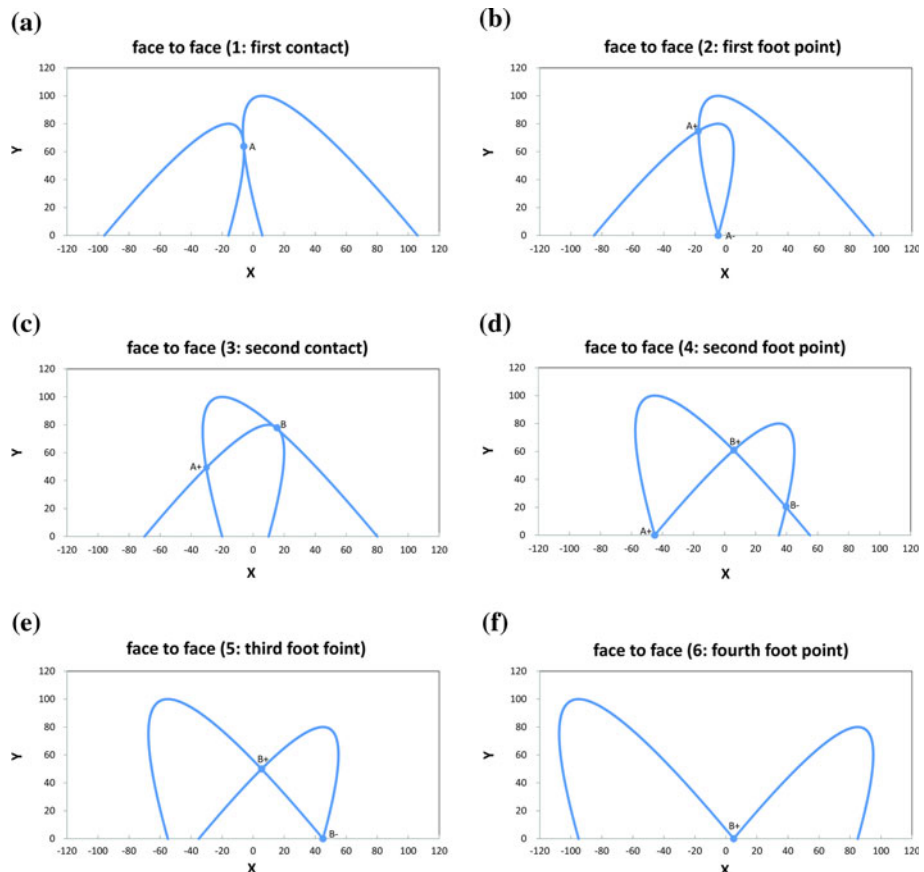


**Fig. 3** Critical phases of intersecting two arches in Case 1A. **a** Phase 1. **b** Phase 2. **c** Phase 3. **d** Phase 4. **e** Phase 5. **f** Phase 6

**Case 1: “face to face”** Snapshots of the surface of section at critical phases of this case are shown in Fig. 3. The corresponding characteristic curve is shown in Fig. 4a. Initially, two arches approach each other. At a certain value of  $a$ , two arches make the first intersection  $A$ , as is shown in Fig. 3a. This intersection is a tangential one which causes a saddle-node bifurcation of periodic orbits. The corresponding point on the characteristic curve is labelled also by  $A$ . Point  $A$  bifurcates into two points  $A_+$  and  $A_-$ , if parameter  $a$  further goes down.

Two forefoot points approach and coincide (Fig. 3b). Point  $A_-$  disappears at triple collision manifold, whereas point  $A_+$  survives this event. Then, the head of the RG-arch tangentially intersects with the hindfoot of the LG-arch at  $B$  (Fig. 3c). It should be noted that periodic points  $A_+$  and  $B$  belongs to different branches of the characteristic curve. Then, the hindfoot of the RG-arch and the forefoot of the LG-arch meet at their footpoints (Fig. 3d). Point  $A_+$  disappears, whereas point  $B_+$  and  $B_-$  survive this phase. Then, the forefoot of the RG-arch and the hindfoot of the LG-arch meet at their foot points (Fig. 3e). Point  $B_-$  disappears, whereas point  $B_+$  survives this phase. Finally, two hindfoot points approach and coincide (Fig. 3f). After that, the intersection  $B_-$  disappears.

The characteristic curve of Case 1B has also two branches, which apparently overlap differently from Case 1A in Fig. 4b. This difference reflects as the order of appearance/

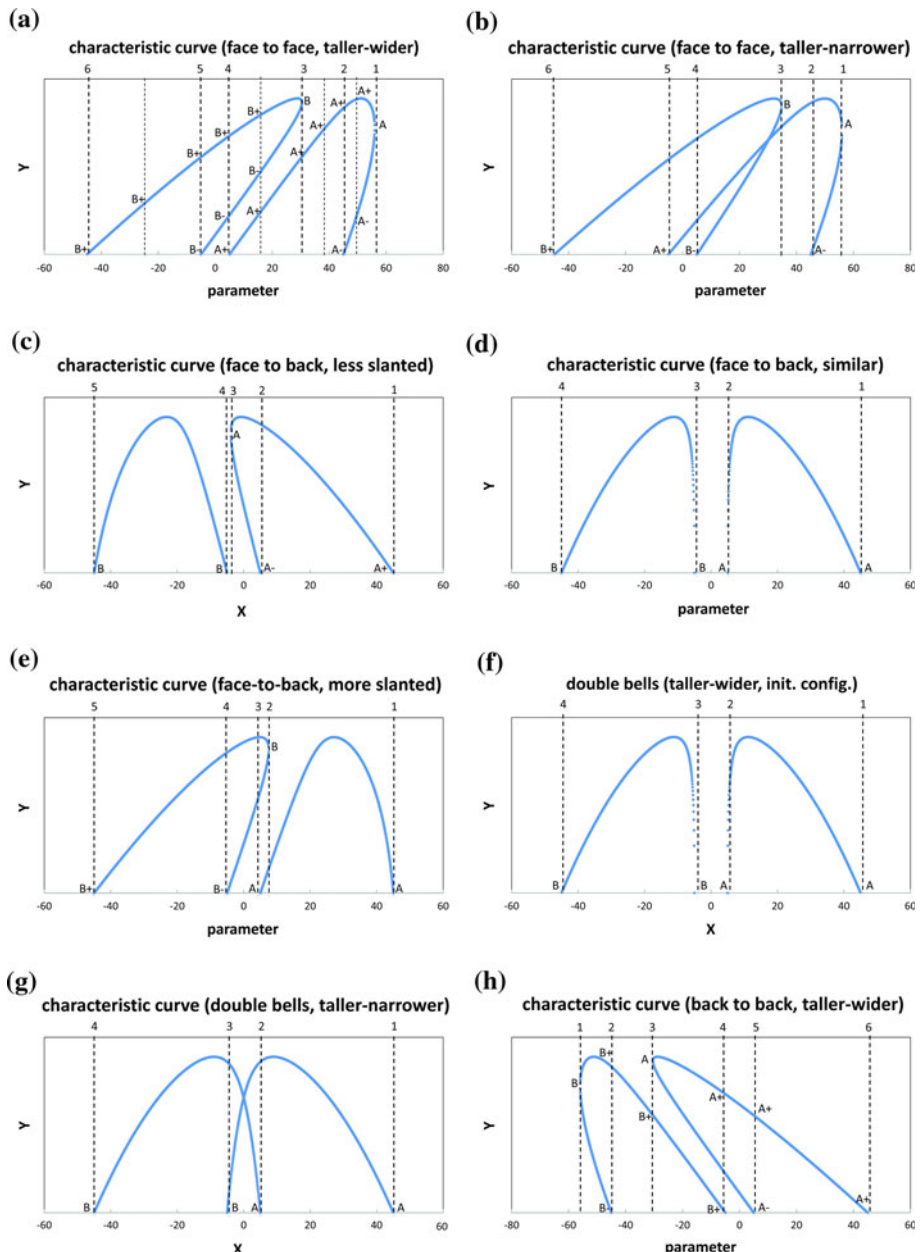


**Fig. 4** Typical characteristic curves of configurations cases Case 1–4. **a** Case 1A. **b** Case 1B. **c** Case 2A. **d** Case 2B. **e** Case 2C. **f** Case 3A. **g** Case 3B. **h** Case 4A

disappearance of periodic points  $A_+$  and  $B$  on the surface of section. Different from the case of total eclipses, there do not necessarily exist four contacts: only the first and second contacts are realised in Cases 1A and 1B.

*Case 2: “face to back”* The case is divided into three sub-cases: 2A (less slanted RG-arch), 2B (geometrically similar two arches), and 2C (more slanted RG-arch), whose characteristic curve are shown in Fig. 4c, d, and e, respectively.

In Case 2A, the second contact realises, that is, points  $A_+$  and  $A_-$  appear in this order and then annihilate.

In Case 2C, the third contact is realised, that is, points  $B_-$  and  $B_+$  appear then annihilate in this order.

Case 2B is very special in the sense that the tangential intersection twice takes place at foot points of arches.

*Case 3: “double bells”* The characteristic curve of this case is shown in Fig. 4f and g. All intersections between the arches take place at their foot points. The order of intersections is the appearance of point A, its disappearance, the appearance of point B, and its disappearance. The combination of height and width also determines whether or not components of characteristic curves have an apparent overlap.

*Case 4: “back to back”* As we have discussed, this case is essentially identical to Case 4. We omit the details and show only the result in Fig. 4h.

## 5 Applicability of results: Cylinder of persistent arches

We briefly explained the structure of the surface of section in §3.2. There we talk about persistent sub-arches which sit in the second lowest positions of the surface (the lowest position is occupied by escape regions, i.e., scallops). In this section, using these persistent arches, we show that we can actually obtain periodic orbits.

Let  $N_{\text{fp}} = N_{\text{fp}}(a_0)$  be the number of foot-points on the  $\theta$ -axis at  $a = a_0$ . Let us then introduce the  $N_{\text{fp}}$  persistent sub-arches:

$$\begin{aligned} R_1 &= [\![ \{ \cdot \cdot 2^j * \mid j < \infty \} ]\!], \dots, \\ R_{2i} &= [\![ \{ \cdot \cdot (21)^i (1)^j * \mid j < \infty \} ]\!], \\ R_{2i+1} &= [\![ \{ \cdot \cdot (21)^i (2)^j * \mid j < \infty \} ]\!], \dots, R_{N_{\text{fp}}}. \end{aligned}$$

We know that sub-arches  $R_i$  ( $i \leq N_{\text{fp}}(a_0)$ ) survive with preserving their alignment order for  $a \leq a_0$ . The same is true with their mirrored intersectable counterparts  $\mathcal{MR}_{N_{\text{fp}}-i}$  and  $\mathcal{MR}_{N_{\text{fp}}-i+1}$ . These properties are assured by the following facts studied in Saito and Tanikawa (2007) and McGehee (1974):

1. Sub-arches  $R_i$  are aligned, from the left to the right, in the ascending order of suffixes  $i$  (Saito and Tanikawa 2007).
2. Sub-arches  $R_i$  has two convergence points on the  $\theta$ -axis, one of which is shared by  $R_{i-1}$  and the other by  $R_{i+1}$  (Saito and Tanikawa 2007). Hence, allocating  $1 + N_{\text{fp}}(a_0)$  foot points on the  $\theta$ -axis, one can relate  $R_i$  with a segment of the  $\theta$ -axis between  $(i-1)$ -th to  $i$ -th foot points. Let us call this a *foot-segment*.
3. There are two fixed points on the triple collision manifold (TCM) (McGehee 1974). Foot points of arches are intersections of their stable and unstable manifolds with the surface of section (Saito and Tanikawa 2007).
4. McGehee’s equations are invariant under  $(\tau, v, w) \mapsto (-\tau, -v, -w)$  and  $(s, w) \mapsto (-s, -w)$  (McGehee 1974). At totally degenerated cases, the stable/unstable manifolds

on the TCM smoothly connect with each other. Therefore, foot-points are symmetrically aligned with respect to  $\theta = 90^\circ$  on the  $\theta$ -axis.

5. Some properties for these manifolds are translated to the following two facts.  $N_{\text{fp}}(a)$  is a monotonically decreasing step function of  $a$ . New foot points are always inserted at  $\theta = 180^\circ$  (namely, at the rightmost position) at totally degenerate cases.

Now, let us follow the change of overlapping of foot-segments and mirrored foot-segments between two degeneracies. Let  $N_{\text{fp}} = m$  be the number of foot-points of initial total degeneracy. Let  $I$  be the serial number of a foot-segment of separated counted up from the leftmost position. Similarly, let  $I'$  be the serial number of a mirrored foot-segment counted from the rightmost position. In the initial state, each foot-segment  $I$  completely overlap with one of the mirrored foot-segment  $I'$  such that  $I + I' = m + 1$ . In the next total degeneracy ( $N_{\text{fp}} = m + 1$ ), the serial numbers of overlapping foot-segments satisfy  $I + I' = m + 2$ . In an intermediate state, each foot-segment  $I$  has common points with two mirrored foot-segments  $I'$  and  $I''$  so that  $I + I' = m + 1$  and  $I + I'' = m + 2$ . Since mirrored persistent arches are

$$\begin{aligned}\widetilde{R}_1 &= \llbracket \{*1^j \cdot * | j < \infty\} \rrbracket, \dots, \\ \widetilde{R}_{2i} &= \llbracket \{*(2)^j (21)^i \cdot * | j < \infty\} \rrbracket, \\ \widetilde{R}_{2i+1} &= \llbracket \{*(1)^j (21)^i \cdot * | j < \infty\} \rrbracket, \dots, R_{N_{\text{fp}}},\end{aligned}$$

intersections  $R_I \cap R_{I'}$  with  $I + I' = m + 1$  or  $I + I' = m + 2$  are non-empty. In order that there exist periodic orbits in these intersections, their symbolic sequence should be periodic.

$$R_I \cap R_{I'} = \llbracket \{*\bar{u}(\tilde{s}_{I'})^{j'}(21)^{\lfloor I'/2 \rfloor} \cdot (21)^{\lfloor I/2 \rfloor} (s_I)^j v *\} \rrbracket,$$

where  $u, v$  are arbitrary words,  $s_I \equiv 1 + (I \bmod 2)$ ,  $\tilde{s}_{I'} \equiv 2 - (I \bmod 2)$ , and  $j', j$  are arbitrary integers. If  $u = (21)^{\lfloor I/2 \rfloor}$ ,  $v = (21)^{\lfloor I'/2 \rfloor}$ ,  $j = j'$ , and  $s_I = \tilde{s}_{I'}$ , then the first past part coincides with the first future part and these part infinitely repeats if Theorem 3.2 is applicable.

We have an example. Let  $m = 4$ ,  $I = 1$ ,  $I' = 4$  then the periodic word  $w_j = (21)^0 2^j (21)^2$  is obtained.  $w_1 = 22121$ ,  $w_2 = 222121$ ,  $w_3 = 2222121$ . This reproduces the result of [Tanikawa and Mikkola \(2000b\)](#).

## 6 Concluding remarks

We have observed that characteristic curves start and end at the triple collision manifold. We are not sure that this is a natural phenomenon from the view point of the Poincaré index. Our surface of section is, in the McGehee's coordinates, the part of  $s = 0$  plane restricted to the inside of the TCM. We expect that the Poincaré index is preserved in the extended map defined over the entire  $s = 0$  plane. This means that there is also one parameter family of periodic points on the part of  $s = 0$  plane outside the TCM and they annihilate with their counterpart coming from the inside part. These hypothetical points correspond not to periodic motions but to oscillatory ones, since the energy is positive outside the TCM.

In the present work, we have restricted ourselves to intersections between persistent arches. Intersections between two regions, appropriately taken from persistent arches, the other arches, germs, and pipelines, also make periodic orbits. In this way, almost all of periodic orbits can be found other than the Schubart and its daughter orbits.

In the case of periodic orbits  $(21121)^\infty \cdot (21121)^\infty$ , the characteristic curve has a vertical portion which implies a saddle-node bifurcation (Paper II). Although this discovery has been

the motivation of the present work, our demonstration in the present paper shows that in general the characteristic curves do not necessarily have such a vertical portion.

## References

- Giorgilli, A., Locatelli, U., Sansotera, M.: Kolmogorov and Nekhoroshev theory for the problem of three bodies. *Celest. Mech. Dyn. Astron.* **104**, 159–173 (2009)
- Gidea, M., Llibre, J.: Symmetric planar central configurations of five bodies: Euler plus two. *Celest. Mech. Dyn. Astron.* **106**, 89–107 (2010)
- Hietarinta, J., Mikkola, S.: Chaos in the one-dimensional gravitational three-body problem. *CHAOS* **3**, 183–203 (1993)
- Kovács, T., Efdi, B.: Transient chaos in the Sitnikov problem. *Celest. Mech. Dyn. Astron.* **105**, 289–304 (2009)
- McGehee, R.: Triple collision in the collinear three body problem. *Inventiones Math.* **27**, 191–227 (1974)
- Mikkola, S., Hietarinta, J.: A numerical investigation of the one-dimensional Newtonian three-body problem. I. *Celest. Mech. Dyn. Astron.* **46**, 1–18 (1989)
- Orlov, V.V., Petrova, A.V., Tanikawa, K., Saito, M.M., Martynova, A.I.: The rectilinear three-body problem. *Celest. Mech. Dyn. Astron.* **100**, 93–120 (2009)
- Saito, M.M., Tanikawa, K.: The rectilinear three-body problem using symbol sequence I. Role of triple collision. *Celest. Mech. Dyn. Astron.* **98**, 95–120 (2007) (Paper I)
- Saito, M.M., Tanikawa, K.: The rectilinear three-body problem using symbol sequence II. Role of the periodic orbits. *Celest. Mech. Dyn. Astron.* **103**, 191–207 (2009) (Paper II)
- Tanikawa, K., Mikkola, J.: Triple collisions in the one-dimensional three-body problem. *Celest. Mech. Dyn. Astron.* **76**, 23–34 (2000a)
- Tanikawa, K., Mikkola, J.: One-dimensional three-body problem via symbolic dynamics. *CHAOS* **10**, 649–657 (2000b)
- Topputo, F., Belbruno, E.: Computation of weak stability boundaries: Sun-Jupiter system. *Celest. Mech. Dyn. Astron.* **105**, 3–17 (2009)